

## Optical Properties of Phthalocyanine and Naphthalocyanine Compounds<sup>†</sup>

Jan Andzelm,\* Adam M. Rawlett, Joshua A. Orlicki, and James F. Snyder

U.S. Army Research Laboratory, Aberdeen Proving Ground, Maryland 21005-5069

Kim K. Baldridge

University of Zurich, 190 Winterthurerstrasse, Zurich CH-8057, Switzerland

Received January 14, 2007

**Abstract:** Phthalocyanines, naphthalocyanines, and their derivatives are frequently used as light modulating materials. These compounds, with their stable planar square structure and highly delocalized  $\pi$ -electron system, are being used in numerous technological applications, such as pigments in chemical sensors, and more recently as photosensitizers for photodynamic therapy. The nonlinear optical properties (NLO) of these compounds are of particular importance. Using density functional method (DFT), we calculated the optical properties of phthalocyanine and naphthalocyanine complexes with Si as a central atom. We examined the effect of hydrophilic axial substituents and the size of polycyclic aromatic hydrocarbons surrounding the porphyrazine-Si kernel on the optical properties of title molecules. Both UV–vis and RSA spectra are calculated and are compared with available experimental results. The time-dependent DFT (TDDFT) with the B3LYP functional predicts that the characteristic UV–vis absorption maxima are blue-shifted; however, the relative error is almost constant for phthalocyanine and naphthalocyanine compounds. The TDDFT triplet–triplet absorption spectra of Si-phthalocyanine and Si-naphthalocyanine complexes reproduce experimental data well.

### 1. Introduction

Phthalocyanines (Pcs), naphthalocyanines (Ncs), and their derivatives have been studied extensively since the beginning of the previous century and have been utilized as dyes and pigments because of their intense blue or green color.<sup>1</sup> In recent years, they have also been used in photocopiers and printers,<sup>2</sup> photovoltaic cells,<sup>3</sup> gas sensors,<sup>4</sup> nonlinear optical limiting devices,<sup>5</sup> photodynamic therapy agents,<sup>6</sup> and many other applications. These chromophores display interesting properties, such as high thermal and chemical stability, efficient light absorption in the red visible wavelengths, and both semi- and photoconducting characteristics. These properties are the result of the stable macrocyclic conjugated network of  $\pi$ -electrons leading to high electrical polarizability

and rapid nonlinear response of the charge density to the applied intense electromagnetic fields.<sup>7</sup> The large nonlinear absorption in the visible spectrum, together with the ultrafast response time and easy processability,<sup>8</sup> make the optical modulation abilities of this class of chromophores of key importance for many applications.

Optical modulation with Pcs was first reported in 1989 for chloroaluminumphthalocyanine,<sup>9</sup> and since then many other Pcs and Ncs with these properties have been identified.<sup>10</sup> This variety of chromophores is attributable to the versatility of the synthetic organic chemistry for such molecules. Through synthetic means, one can alter the physical properties (e.g., steric and electronic) of the system by selecting specific coordinating central atoms, attaching various moieties to the exterior ring system, and substituting the ligands on the coordinating central atom.<sup>10–12</sup>

The optical modulation properties of chromophores can be explained by a reverse saturable absorption (RSA)

<sup>†</sup> Dedicated to Professor Dennis R. Salahub on the occasion of his 60th birthday.

\* Corresponding author e-mail: jandzelm@arl.army.mil.

mechanism.<sup>11</sup> RSA is essentially a sequential two-photon absorption leading to population of excited triplet states of a material by way of first reaching the excited singlet state. The optimal RSA material would have an excited triplet–triplet cross-section much larger than the cross-section of the ground to first excited singlet–singlet transitions. The intersystem crossing from the lowest singlet excited-state to the lowest triplet excited-state must also be allowed, and the excited-state must have a reasonably long lifetime.<sup>11</sup> A practical optical device would require a high concentration of soluble RSA material in the optical beam potentially leading to undesired intermolecular interactions (aggregation). This phenomenon may be alleviated through the use of chromophores with axial substituents that disrupt the favored crystal packing of the unsubstituted chromophore. The use of water as a solvent leads to stacking Pcs, which significantly affects the optical spectra and degrades their optical modulating capabilities.<sup>13,14</sup> Various axial substituents have been used to minimize the intermolecular stacking of chromophores in water. Huang et al.<sup>15</sup> have used long axial poly(ethylene glycol) (PEG) chains, while Dominguez et al.<sup>16</sup> have synthesized the polyethyleneoxide-capped Pcs.

In this paper we investigate optical absorption as a function of axial substituents in Pcs and Ncs, with silicon as the central atom. In the case of SiPc, hydrophilic substituents such as poly(ethylene oxide) (PEG) oligomers are chosen because they promote water solubility of the system.<sup>13,15</sup> In the case of SiNc, we select the SINC molecule<sup>12</sup> and also propose other substituents for Ncs. Both visible (UV–vis) and nonlinear (RSA) absorption are studied using quantum chemistry methods. The calculated spectra are compared with the published experimental measurements of the ground-state absorption spectra<sup>12,13,15–19</sup> and the transient absorption spectra due to the triplet–triplet excitations.<sup>20–23</sup>

Molecular systems under investigation, particularly in the stacking conformation of the molecules, can involve more than 200 atoms. This requires use of the computationally efficient quantum techniques such as density functional theory (DFT) or semiempirical methods that are computationally less demanding than traditional *ab initio* methods. The need for efficient calculations of optical spectra is paramount, as recently synthesized optically active complexes may involve very large binuclear conjugated-Pc structures,<sup>24</sup> dendritic phthalocyanines,<sup>13</sup> or conjugated carotenoid pigments.<sup>25</sup> Therefore, developing fast DFT methods as pioneered by Dunlap,<sup>26</sup> Baerends,<sup>27</sup> and Salahub<sup>28</sup> is of critical importance for successful study of Pc and Nc compounds. These methods approximate electron density and therefore can be used only with the local or gradient corrected Hamiltonian. Therefore, we also use the GGA DFT method in addition to the B3LYP method that is commonly used in calculations for chromophores.

Calculations of absorption spectra were accomplished in the present work using the time-dependent density functional theory (TDDFT)<sup>29,30</sup> method. This method has been previously shown to provide reasonable predictions for phthalocyanines and metallophthalocyanines structures and UV–vis absorption.<sup>31–37</sup> While the TD-DFT study of UV–vis spectra requires calculation of singlet–singlet excitations (S–

S), predicting RSA requires calculation of triplet–triplet (T–T) absorption and ultimately excited singlet–triplet cross-section. In this paper we will refer to T–T absorption spectrum as a RSA spectrum. A few investigations have explored excited triplet states for zinc phthalocyanine<sup>32</sup> and zinc porphyrin<sup>23,38</sup> as well as meso-diaryloctaalkyl porphyrins.<sup>39</sup> The most relevant for this work is experimental study of the T–T transitions in the SINC molecule<sup>12,20</sup> and also in silicon phthalocyanines with axial siloxy ligands.<sup>21,22</sup>

Understanding the mechanism of UV–vis excitations is facilitated by considering the two primary excitation peaks of porphyrins: the Q band in visible range and the B (or Soret) band in the UV region, as has been explained by the “four-orbital model” first introduced in 1963 by Gouterman.<sup>40</sup> According to this model, the Q band originates from electron excitations out of the HOMO and into the LUMO and LUMO+1, while the B band is from transitions from HOMO-1 to LUMO and LUMO+1. Subsequent studies proposed a more detailed explanation involving more than “four orbitals” because the quasi-degeneracy of orbitals close to the HOMO is removed.<sup>41</sup> The character of UV–vis spectra was studied in detail for porphyrin, porphyrazine,<sup>42</sup> and metallophthalocyanine<sup>32</sup> complexes.

## 2. Computational Methods

The structures of all molecular systems were calculated using the Dmol,<sup>43</sup> GAMESS,<sup>44</sup> and Gaussian03<sup>45</sup> software. Initially, structures were optimized using the PBE<sup>46</sup> DFT functional with the double numerical basis set, DNP,<sup>47</sup> using DMol. In order to validate the completeness of the basis set, several structures were also investigated using the 6-31G(d), 6-311G(d), 6-311G(d,p), and 6-311+G(d) basis sets.<sup>48</sup> The excited states were calculated with the hybrid DFT functional B3LYP<sup>49</sup> within the TDDFT methodology as implemented in the Gaussian03 program.<sup>50</sup> The UV–vis spectrum was predicted from singlet–singlet excitations, while the RSA spectrum was calculated from the triplet–triplet transitions. The open-shell DFT calculations for the triplets were carried out using the unrestricted Kohn–Sham spin-density approach. The  $\langle S^2 \rangle$  values for all triplet states are below 2.04, indicating low spin contamination, a typical feature of the open-shell DFT calculations.<sup>51</sup> The B3LYP Hamiltonian was proven to provide accurate structures and reasonable UV–vis spectra for a variety of chromophores.<sup>23,31–37,52–54</sup> We have also used the gradient corrected functional PBE because it allows for computationally efficient implementation that is of key importance for this study of large chromophores.<sup>26–28</sup> In order to improve the efficiency of calculations, we have also imposed the symmetry of the chosen structures and applied fitting functions in the case of gradient corrected DFT functional. We have used the PBE functional to calculate structures of molecular systems. The RSA spectrum was calculated using the singlet ground state and the first triplet excited-state geometries, and we will refer to these levels of calculations as vertical and adiabatic spectra, respectively. The UV–vis spectra were compared with results of the configuration interaction method using single excitations (CIS) within the semiempirical ZINDO/INDO2 method.<sup>55</sup> It was recently reported for several metal-phthalocyanine

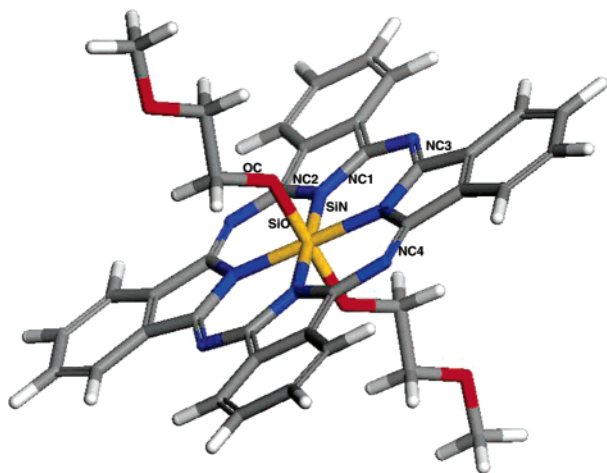


**Figure 1.** Structure of SiPc-(PEG<sub>75</sub>)<sub>2</sub>.

complexes that the Q-band absorption peaks predicted by ZINDO are in better agreement with the experimental results as compared to the TDDFT calculations.<sup>56</sup> The ZINDO method was also successfully used to compare electronic properties of zinc phthalocyanine and helicenocyanine.<sup>57</sup> Considerations of atomic populations were performed using the Hirshfeld population analysis (HPA)<sup>58</sup> and the popular, Mulliken population analysis (MPA).<sup>59</sup> Conceptual advantage of HPA over that of MPA was recently discussed by Roy et al.<sup>60</sup>

### 3. Results

Structures and spectra of SiPc complexes with axially bonded PEG polymers were studied first and compared with the recent experimental measurements. Subsequently results for the SiNc compound with various axial substituents on the central Si atom were investigated. The complete sets of Cartesian coordinates are available upon request.

**3.1. Structures and Spectra of SiPc-PEG.** The SiPc-PEG complexes are of central interest in this paper because of their solubility in water and their desirable UV–vis and RSA properties. The axial site substitution prevents cofacial aggregation: this was found by attaching PEG polymer<sup>15</sup> or the dendritic fragments to the silicon-containing Pc.<sup>16</sup> This axial modification did not affect the characteristic Q-absorption maximum that was found to be at range of 676–685 nm.<sup>13,15,16</sup> We have confirmed that the DFT method predicts the sharp Q band regardless of the length or conformations of the PEG polymer attached to central atom in the SiPc-PEG complex.<sup>61</sup> No significant differences in the SiPc ring structure were noted, and the UV–vis spectra show quite similar location of the main Q and B excitation bands.<sup>61</sup>

In this paper, we studied the structure and excited states of the SiPc-PEG compound using various levels of theory. A simple SiPc-(PEG<sub>75</sub>)<sub>2</sub> structure (Figure 1) was chosen because other conformations exhibit similar optical properties. The structure was optimized for a singlet and a triplet state assuming the  $C_{2h}$  symmetry of the complex. Table 1 shows several structural parameters of the SiPc-(PEG<sub>75</sub>)<sub>2</sub> complex as a function of methodology used. Across all methods investigated, we note that the structural parameters are within 0.01 Å and 3 deg for bonds and angles,

respectively. Choosing the DFT functional appears to affect the results more than the choice of basis set. The hybrid functional B3LYP predicts contraction of the Pc ring (i.e., shorter SiN, NC, and N=C bonds), while the most widely used gradient-corrected functional, PBE, predicts expansion of the PC ring. The axially inserted PEG appears to be closer to the silicon atom using the hybrid functional than predicted with the GGA functional, a feature predicted regardless of the basis set used. The SiOC angle is 130 deg on average. Improving the basis set causes only a small change (increase) in the SiOC angle. Compared with experimental data<sup>62</sup> we find an exceptionally good performance of the B3LYP/6-31G(d) approach for the N–C distances of the phthalocyanine planar ring. The discrepancy of 0.04 Å in SiO distances can be attributed to a different ligand connected with oxygen atoms used in our calculations, compared to the one used in the experiment. Since the selected geometry parameters in Table 1 do not include a hydrogen atom, it is sufficient to use single polarization function located only on heavy atoms. Using diffuse functions insignificantly affects the geometry of the planar phthalocyanine ring for the singlet and triplet excited states.

The excitation of one electron from HOMO ( $a_u$ ) to LUMO ( $a_g$ ) gives rise to a  $^3A_u$  excited-state within the  $C_{2h}$  symmetry. The most noticeable structural changes upon going from ground-state singlet,  $S_0$ , to first triplet state,  $T_1$  (Table 1), are the distortions of N–C bonds and enlargement of the SiO bond distance. Energetically,  $T_1$  is located 0.94 eV above  $S_0$ . This adiabatic transition calculated at the B3LYP/6-31G(d) level appears to be converged because the  $S_0 \rightarrow T_1$  splitting at the B3LYP/6-311+G(d,p) level is 0.98 eV. The vertical transition calculated at the B3LYP/6-31G(d) level is 1.01 eV, indicating that the effect of structure optimization is more pronounced than the improvements in basis set. The calculated excitation energy of about 1.0 eV compares well with the 1.13–1.14 eV determined from the phosphorescence spectra in chloronaphthalene as reported by Ricciardi et al.<sup>32</sup>

Table 2 summarizes computational predictions of the UV–vis and RSA spectra as a function of the methods employed. The choice of structure and method appears to have a more pronounced effect on spectra than in the case of geometry prediction. The Q and RSA band are more sensitive than the B band. We found that using the PBE- or B3LYP-optimized structure affects the spectra slightly, at most by 10 nm. A similar effect can be seen with the increase of the basis set. A better description of hydrogen atoms, through the use of the p polarization function, seems unimportant, confirming that the main absorption bands originate from the  $\pi \rightarrow \pi$  transitions of the phthalocyanine core. The use of singlet-optimized structures in calculating triplet excited states can red-shift the RSA band by up to 20 nm. Comparison with experimental data confirms the well-known significant blue-shift of the UV–vis spectrum.<sup>15,53,54,56</sup> The Q and B bands are shifted by about 70 and 20 nm, respectively. The triplet–triplet absorption spectrum is composed of three major excitations centered around 500 nm. This is very close to a maximum of broad absorption centered at ~495 nm found from transient absorption spectra attributed to the triplet absorption band.<sup>21,22</sup>

**Table 1.** Comparison of Structural Parameters of SiPc-(PEG<sub>75</sub>)<sub>2</sub> for Various Levels of DFT Theory and Basis Set<sup>b</sup>

	X-ray data <sup>a</sup>	singlet PBE/DNP	B3LYP/		triplet PBE/DNP	B3LYP/	
			6-31G(d)	6-311+G(d,p)		6-31G(d)	6-311+G(d,p)
SiN	1.92	1.944	1.943	1.943	1.940	1.939	1.939
NC1	1.375	1.383	1.378	1.377	1.372	1.363	1.361
NC2	1.375	1.383	1.378	1.377	1.404	1.404	1.402
NC3	1.321	1.324	1.321	1.319	1.331	1.329	1.327
NC4	1.321	1.324	1.321	1.319	1.321	1.318	1.315
SiO	1.68	1.729	1.724	1.723	1.736	1.731	1.730
CO		1.414	1.406	1.408	1.413	1.405	1.407
SiOC		128.4	130.0	130.9	127.7	129.5	130.4

<sup>a</sup> For SiPc(OSiMe<sub>3</sub>)<sub>2</sub> from ref 62. <sup>b</sup> See Figure 1 for the definition of structural parameters. Distances are in Å, angles are in deg.

**Table 2.** Comparison of Main UV–Vis Excitation Energies (in nm) and Oscillator Strengths (*f*) for SiPc-(PEG<sub>75</sub>)<sub>2</sub><sup>e</sup>

	Q		B	
Singlet–Singlet Transitions				
experiment <sup>a</sup>	677		354	
B3LYP/6-31G(d) <sup>b</sup>	604(0.37)	592(0.37)	335(0.32)	334(0.44)
B3LYP/6-31G(d)	613(0.37)	600(0.36)	338(0.50)	336(0.54)
B3LYP/6-31G(d,p)	612(0.37)	600(0.36)	337(0.64)	335(0.55)
B3LYP/6-311G(d)	618(0.38)	605(0.37)	338(0.58)	337(0.53)
Triplet–Triplet Transitions				
experiment <sup>c</sup>	495			
B3LYP/6-31G(d) <sup>b</sup>	595(0.10)	515(0.24)	492(0.30)	463(0.25)
B3LYP/6-311G(d) <sup>b</sup>	598(0.08)	517(0.22)	497(0.21)	469(0.32)
B3LYP/6-31G(d) <sup>d</sup>	619(0.12)	526(0.24)	509(0.21)	478(0.31)
B3LYP/6-311G(d) <sup>d</sup>	622(0.14)	526(0.24)	516(0.11)	488(0.20)
B3LYP/6-31G(d)	605(0.10)	522(0.18)	499(0.29)	468(0.26)
B3LYP/6-311G(d)	607(0.11)	522(0.25)	504(0.19)	
B3LYP/6-31G(d,p)	605(0.10)	522(0.15)	499(0.27)	469(0.28)

<sup>a</sup> For SiPc-(PEG<sub>550</sub>)<sub>2</sub> from ref 15. <sup>b</sup> Using B3LYP/6-311+G(d) optimized structure. <sup>c</sup> A broad absorption centered at ~495 nm is assigned to the triplet absorption for SiPc-(X)<sub>2</sub> where X are various axially bonded siloxy ligands.<sup>21,22</sup> <sup>d</sup> PBE/DNP singlet optimized structure was used. <sup>e</sup> The PBE/DNP structure was used unless specified otherwise.

The character of the investigated singlet–singlet transitions was found to follow approximately the Goutermann's assignments, as observed by the data shown in Table 3. The Q band arises from  $\pi$  transitions from occupied to unoccupied orbitals. The largest contribution to Q excitations comes from HOMO to LUMO and LUMO+1 excitations. These  $\pi$  orbitals are localized in the plane of a phthalocyanine ring. There is also a small contribution from lower occupied orbitals HOMO-6 (*b<sub>u</sub>*). This orbital has a significant contribution from  $\pi$  orbitals of PEG's oxygen atom. The B band excitations can be interpreted as excitations from several levels below HOMO to LUMO and LUMO+1 levels. The low lying levels such as HOMO-6 to HOMO-13, both of *b<sub>u</sub>* symmetry, have significant contributions from  $\pi$  orbitals of PEG's oxygen atom. Level HOMO-8 (*a<sub>u</sub>*) has only a small ligand contribution, and the HOMO-11 (*b<sub>g</sub>*) is localized far from the center of the Pc structure. It is interesting that none of the major orbitals contributing to the Q or the B band are significantly affected by the central silicon atom.

The character of transitions in the triplet–triplet spectrum is also presented in Table 3. The  $\pi$  spin orbitals close to the

**Table 3.** B3LYP/6-31G(d) Calculated Major Excitation Energies ( $\Delta E$  in nm)<sup>a</sup> and Oscillator Strengths (*f*) for the SiPc-(PEG<sub>75</sub>)<sub>2</sub> Complex at *C<sub>2h</sub>* Symmetry

$\Delta E$	<i>f</i>	transition	weight <sup>b</sup>	symmetry
		Singlet→Singlet		
		H→L	0.603	A <sub>u</sub>
		H-6→L+1	0.232	
604	0.370	H→L+1	0.606	B <sub>u</sub>
		H-6→L	0.240	
592	0.367	H-6→L	0.503	B <sub>u</sub>
		H-13→L	0.292	
		H-11→L	0.216	
335	0.318	H-11→L	0.587	B <sub>u</sub>
		H-8→L	0.227	
		H-6→L	0.176	
334	0.371	H-6→L+1	0.463	A <sub>u</sub>
		H-8→L+1	0.358	
		H-13→L+1	0.311	
333	0.436	H-13→L	0.616	B <sub>u</sub>
		H-6→L	0.218	
322	0.103	H-13→L+1	0.564	A <sub>u</sub>
		H-6→L+1	0.277	
320	0.174	H→L+4	0.655	A <sub>u</sub>
		H-11→L+1	0.134	
		Triplet→Triplet		
		H→L+1 ( $\alpha$ )	0.687	B <sub>u</sub>
		H-9→L ( $\beta$ )	0.532	
595	0.096	H-7→L ( $\beta$ )	0.820	A <sub>u</sub>
		H→L+2 ( $\alpha$ )	0.358	
515	0.245	H-9→L ( $\beta$ )	0.662	B <sub>u</sub>
		H→L+5 ( $\alpha$ )	0.570	
492	0.304	H→L+5 ( $\alpha$ )	0.790	B <sub>u</sub>
		H-9→L ( $\beta$ )	0.457	
463	0.254			

<sup>a</sup> Transitions with oscillator strength (*f*) of 0.1 or larger are shown.

<sup>b</sup> The absolute values of weights for major transitions are presented.

HOMO levels in both spin manifolds ( $\alpha$  and  $\beta$ ) are localized within the phthalocyanine plane. However the HOMO-7 and HOMO-9  $\beta$  spin orbitals have some contribution from the oxygen atom of the PEG ligand. Apparently, the ligand effect on the RSA spectrum is not significant, which was also observed in studies of silicon phthalocyanines various axially bonded siloxy ligands.<sup>21,22</sup>

**3.2. Structures and Spectra of SiNc.** Structures of SiNc, SiNc-(OSi(CH<sub>3</sub>)<sub>3</sub>)<sub>2</sub>, and SiNc-(OH)<sub>2</sub> complexes have been optimized using the PBE/DNP level of theory (Figure 2;



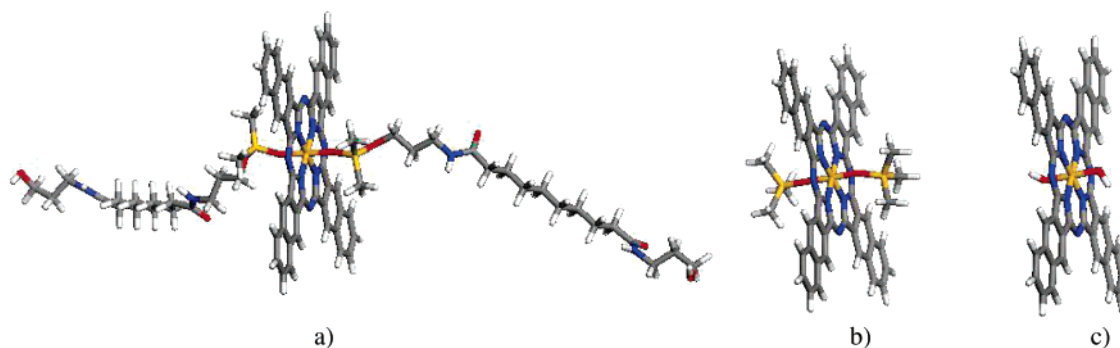


**Figure 2.** Structure of (a) SINC, (b) SiNc-(OSi(CH<sub>3</sub>)<sub>3</sub>)<sub>2</sub>, and (c) SiNc-(OH)<sub>2</sub>.

**Table 4.** Comparison of Main UV–Vis Excitation Energies ( $\Delta E$  in nm) and Oscillator Strengths ( $f$ ) for SINC, SiNc-(OSi(CH<sub>3</sub>)<sub>3</sub>)<sub>2</sub>, and SiNc-(OH)<sub>2</sub> Obtained at the B3LYP/6-31G(d)//PBE/DNP Level

band	SINC <sup>a</sup>	SiNc-(OSi(CH <sub>3</sub> ) <sub>3</sub> ) <sub>2</sub>	SiNc-(OH) <sub>2</sub>	SiNc-(OH) <sub>2</sub> <sup>b</sup>
Q	717(0.51)	711(0.53)	713(0.56)	722(0.57)
	715(0.50)	709(0.53)	708(0.55)	717(0.56)
B	431(0.20)	429(0.26)	430(0.20)	433(0.15)
	429(0.17)	428(0.25)	429(0.25)	432(0.23)
	348(0.35)	346(0.39)	348(0.44)	350(0.43)
	347(0.36)	345(0.40)	347(0.36)	349(0.37)
	327(0.51)	326(0.56)	329(0.49)	330(0.52)
	326(0.53)	325(0.57)	328(0.55)	329(0.42)

<sup>a</sup> Experimental data for SINC molecule are 778 and 335 nm for the Q and B excitation, respectively.<sup>12</sup> <sup>b</sup> Spectra calculated at the B3LYP/6-311G(d)//PBE/DNP level.

geometry is available as Supporting Information). In the case of SiNc-(OH)<sub>2</sub>, both the *C*<sub>1</sub> and *C*<sub>2h</sub> symmetries were applied. The main structural difference occurs in the dihedral angle involving the position of the hydroxyl group above the SiNc ring. The energy difference between the two structures is about 0.6 kcal/mol, thus, quite insignificant. Table 4 lists B3LYP/6-31G(d)//PBE/DNP primary excitation energies for the SiNc system when various axial substituents are considered. Increasing the basis set to 6-311G(d) causes a minor red shift in the spectra, the largest shift occurring for the Q band at about 8 nm. The three spectra are almost identical, indicating that the nearest environment of the SiNc ring determines the optical properties. The primary geometrical features of the complexes, such as Si–N, are all within 0.01 Å. The central Si–O distance for SINC and SiNc-(OSi(CH<sub>3</sub>)<sub>3</sub>)<sub>2</sub> are within 0.01 Å, while the Si–O bond length in the case of the SiNc-(OH)<sub>2</sub> complex is slightly longer, at 0.02 Å.

According to the HPA (MPA), the net charge on the central Si atom is 0.435 (2.068), 0.433 (1.792), and 0.412 (1.788) for SINC, SiNc-(OSi(CH<sub>3</sub>)<sub>3</sub>)<sub>2</sub>, and SiNc-(OH)<sub>2</sub> complexes, respectively. Both population analysis schemes indicate a similar electronic environment of the central Si atom for all SiNc complexes considered in this paper.

Experimental data<sup>12</sup> involving SINC dissolved in dimethylformamide (DMF) shows a Q band centered at 778 nm, followed by a transparent region (500–600 nm) and a B (Soret) band located near 335 nm. The characteristic UV–vis absorption maxima of the Q band,  $\Lambda_{\text{max}}$ , for SiNc-(OH)<sub>2</sub>

and SiNc[OSi(n-C<sub>6</sub>H<sub>13</sub>)<sub>3</sub>]<sub>2</sub> compounds were reported at about 772 nm.<sup>63</sup> Spectra calculated at the B3LYP/631G(d) level confirm quite well the experimental position of the B band and the extent of the transparent region (Table 4). However, the Q band is significantly blue-shifted, compared to the experimental data.

All results discussed to this point were obtained in the gas phase and therefore cannot be directly compared with the experimental data. The effect of the solvent, also being systematically analyzed by this group,<sup>61</sup> can be estimated by including explicit water molecules in the calculations for the SiPc-(PEG<sub>75</sub>)<sub>2</sub> compound. In that case, one observes a small red-shift in the Q band of about 13 nm. A similar effect was recently reported in calculations on the aqueous environment of porphyrazine<sup>64</sup> using the continuum C-PCM method of solvation. Since the DMF solvent has a dielectric constant of about half that of water, we can expect a much smaller solvent effect in the case of SINC.

Calculations of spectra for the SINC molecule, consisting of 207 atoms, require significant computational resources, particularly if, in addition to UV–vis spectra, calculation of RSA spectra arising from triplet–triplet excitations is performed. It was already noticed that the semiempirical method ZINDO<sup>55–57</sup> provides a nonexpensive alternative to the calculation of optical properties. Applying the ZINDO method with INDO/2 parametrization we calculated two main excitations at 772 and 768 nm that can be assigned to the Q band. The calculated B band is composed of four major excitations in the range of 353–329 nm. It is apparent that the ZINDO-calculated Q and B bands coincide with experimentally known spectra.

The character of transitions for the major excitation energies of SiNc-(OSi(CH<sub>3</sub>)<sub>3</sub>)<sub>2</sub> are presented in Table 5. Similarly to the SiPc-(PEG<sub>75</sub>)<sub>2</sub> transitions, (Table 3) the Q band arises from  $\pi$  excitations, mainly from HOMO to LUMO and LUMO+1. These  $\pi$  orbitals are localized in the plane of a naphthalocyanine ring. There is also a small contribution from the lower occupied orbitals HOMO-8. This orbital has significant contribution from the  $\pi$  orbitals of the ligand's oxygen atom. The B band excitations can be interpreted as excitations from several levels below HOMO to LUMO and LUMO+1 levels. The low lying levels such as HOMO-6 to HOMO-11 have significant contributions from the  $\pi$  orbitals of the ligand's oxygen atom.

The character of transitions in the triplet–triplet spectrum

**Table 5.** B3LYP/6-31G(d) Calculated Major Excitation Energies ( $\Delta E$  in nm)<sup>a</sup> and Oscillator Strengths ( $f$ ) for SiNc-(OSi(CH<sub>3</sub>)<sub>3</sub>)<sub>2</sub>

$\Delta E$	$f$	transition	weight <sup>b</sup>
Singlet→Singlet			
711	0.528	H→L	0.609
		H-8→L+1	0.127
709	0.527	H→L+1	0.610
		H-8→L	0.128
429	0.258	H-1→L	0.564
		H→L+4	0.298
428	0.256	H-1→L+1	0.579
		H→L+5	0.284
346	0.395	H-8→L	0.472
		H-7→L+1	0.345
346	0.391	H-8→L+1	0.480
		H-8→L	0.292
326	0.563	H-10→L	0.382
		H-6→L+1	0.307
		H-8→L	0.262
325	0.570	H-10→L+1	0.363
		H-6→L	0.288
		H-8→L+1	0.280
		H-11→L+1	0.244
Triplet→Triplet			
693	0.307	H→L ( $\beta$ )	0.885
656	0.128	H→L+5 ( $\alpha$ )	0.595
		H-2→L ( $\beta$ )	0.581
587	0.335	H-4→L ( $\beta$ )	0.703
		H→L +5 ( $\alpha$ )	0.493
573	0.505	H-4→L ( $\beta$ )	0.562
		H→L+5 ( $\alpha$ )	0.505

<sup>a</sup> Transitions with oscillator strength ( $f$ ) of 0.1 or larger are shown.<sup>b</sup> The absolute values of weights for major transitions are presented.

is also analyzed in Table 5. The  $\pi$  spin orbitals close to the HOMO levels in both spin manifolds are localized within the naphthalocyanine ring. However the HOMO-4  $\beta$  spin orbital has some contribution from the oxygen atom of the ligand's oxygen atom. The main RSA bands of the triplet-triplet spectra calculated here at 573 and 587 nm are very close to these found in laser-induced transient absorptions in the SINC compound.<sup>20</sup> It was reported that the triplet-triplet absorption spectrum has a maximum between 590 and 595 nm.<sup>20</sup>

#### 4. Concluding Remarks

In this paper we have calculated optical properties of phthalocyanine and naphthalocyanine complexes with Si as a central atom. The calculated singlet-singlet excitations were compared with experimentally determined UV-vis spectra.<sup>15-19,22</sup> The triplet-triplet excitations can be induced by pulsed laser excitations, and they are known to decay with time.<sup>20-22</sup> A good RSA molecule should exhibit strong  $T_1 \rightarrow T_N$  excitations in the transparent region of the spectrum that is bracketed by the B band in the blue region and the Q band in the red region of the UV-vis spectrum.<sup>11</sup> By comparing the relative positions of major excitations from the UV-vis and RSA spectra, we can confirm that both silicon-phthalocyanine and -naphthalocyanine compounds

studied in this paper are strong RSA molecules. They offer a transparency in the preferable visual region while exhibiting a strong triplet-triplet absorption band centered between the major Q and B bands of the UV-vis spectrum.

The TDDFT with the B3LYP functional and the 6-31G(d) basis set predicts that the characteristic UV-vis absorption maxima of the Q band,  $\Lambda_{\max}$ , are blue-shifted by about 70 nm, compared to the experimental data.<sup>53,54,56</sup> The TDDFT method better predicts the position of the B band, with the major peaks appearing at about 330 nm, which is in good agreement with the experiment. Also, the TDDFT-calculated triplet-triplet absorption spectra of Si-phthalocyanine and Si-naphthalocyanine complexes reproduces experimental data very well.<sup>20-22</sup> The main peaks of the B and RSA bands are calculated within 20 nm of experimental data.

We found that using PBE-optimized geometry, followed by absorption spectra calculations with B3LYP, may result in a small blue-shift of the Q and RSA band by, at most, 10 nm. This is a useful finding because geometry calculations at the GGA level can be performed more efficiently than they can be with a hybrid functional.<sup>26-28,43</sup> In agreement with earlier reports,<sup>56,57</sup> we also found that using the ZINDO approach at the DFT-optimized geometry results in the large red-shift of the Q-band position and significant improvement of calculated results as compared with experimental data.

The effect of using triplet-optimized structures in predicting  $T_1 \rightarrow T_N$  excitations was also investigated. The vertical  $S_0 \rightarrow T_1$  splitting was calculated at 1.01 and 0.81 eV for SiPc-(PEG<sub>75</sub>)<sub>2</sub> and SiNc-(OSi(CH<sub>3</sub>)<sub>3</sub>)<sub>2</sub>, respectively. The adiabatic splitting was not much different at 0.98 and 0.77 eV, respectively. The calculated values compare reasonably well with reported experimental data of 1.13 and 0.93 eV for the phthalocyanine<sup>32</sup> and naphthalocyanine<sup>20</sup> complexes, respectively. The position of main peaks in the RSA spectrum changed by about 20 nm by using the adiabatic vs vertical approach.

In agreement with experimental reports, the TDDFT/B3LYP approach confirms the small effect on spectra of axial substituents for silicon-phthalocyanine and naphthalocyanine compounds.<sup>15,22</sup> The major effect on spectra occurs with increased linear benzoannulation of porphyrazine. It is well-known that the Q and RSA bands become red-shifted in going from the Pc to Nc compounds.<sup>17-19,23,63</sup> The HOMO level is destabilized, and, consequently, the band gap decreases.<sup>65</sup> Present calculations clearly reproduce this effect, with the band gap decreasing from about 1.4 to 1.1 eV, respectively. The TDDFT/B3LYP calculations lead to an almost constant error in  $\Lambda_{\max}$  of about 70 and 60 nm for the silicon-phthalocyanine and naphthalocyanine compounds.

Results of this investigation improve our understanding of the role of axial substituents for phthalocyanine and naphthalocyanine compounds and provide validation for the TDDFT approach that can be used for prediction of optical properties of larger Nc compounds. Additional, such studies can aid in synthetic possibilities for naphthalocyanine complexes having desirable optical properties.

**Acknowledgment.** The authors are indebted to Andrew G. Mott, Robert C. Hoffman, Timothy M. Pritchett, and

Michael J. Ferry for intellectual discussions and insight into this research. Computational resources of ARL and ASC MSRC are gratefully acknowledged. K.K.B. is grateful to the Swiss National Science Foundation for support of this research.

**Supporting Information Available:** Tables of optimized atomic coordinates for the SiNc species. This material is available free of charge via the Internet at <http://pubs.acs.org>.

## References

- (1) Erk, P.; Hengelsberg, In *The Porphyrin Handbook*; Kadish, K. M., Smith, K. M., Guillard, R., Eds.; Elsevier Science: Amsterdam, 2003; Vol. 19, pp 105–150.
- (2) Gregory, P. *Porphyrins Phthalocyanines* **2000**, 4, 432.
- (3) Eichhorn, H. J. *Porphyrins Phthalocyanines* **2000**, 4, 88.
- (4) Sadaoka, Y.; Gopel, T. A.; Jones, W. *Sens. Actuators, B* **1990**, 1, 148.
- (5) Flom, S. R. In *The Porphyrin Handbook*; Kadish, K. M., Smith, K. M., Guillard, R., Eds.; Elsevier Science: Amsterdam, 2003; Vol. 19, pp 179–190.
- (6) Hasrar, H.; van Lier, J. E. *Chem. Rev.* **1999**, 99, 2379.
- (7) Sheehy, B.; Di Mauro, L. F. *Ann. Rev. Phys. Chem.* **1996**, 47, 463–494.
- (8) Mckeown, N. B. *Phthalocyanine Materials: Synthesis, Structure and Function*; Cambridge University Press: 1998.
- (9) Coulter, D. R.; Miskowski, V. M.; Perry, J. W.; Wei, T. H.; Stryland, E. W. V.; Hagan, D. J. In *Materials for Optical Switches, Isolators and Limiters; Proceedings of SPIE*; 1989; Vol. 1105, pp 42–52.
- (10) Torre, G.; Vazquez, P.; Agullo-Lopez, F.; Torres, T. *Chem. Rev.* **2004**, 104, 3723–3750.
- (11) Perry, J. W. In *Nonlinear Optics of Organic Molecules and Polymers*; Nalwa, H. S., Miyata, S., Eds.; CRC Press: Boca Raton, FL, 1997; pp 813–840.
- (12) Wang, N. Q.; Cai, Y. M.; Heflin, J. R.; Wu, J. W.; Rodenberger, D. C.; Garito, A. F. In *Sol-Gel Optics; Proceedings of SPIE*; 1990; Vol. 1328, pp 100–107.
- (13) Ngai, T.; Zhang, G.; Li, X.; Ng, D. K. P.; Wu, C. *Langmuir* **2001**, 17, 1381–1383.
- (14) Shirk, J. S.; Pong, R. G. S.; Flom, S. R.; Heckmann, H.; Hanack, M. *J. Phys. Chem. A* **2000**, 104, 1438–1449.
- (15) Huang, J.-D.; Wang, S.; Lo, P.-C.; Fong, W.-P.; Ko, W.-H.; Ng, D. K. P. *New. J. Chem.* **2004**, 28, 348–354.
- (16) Dominguez, D. D.; Snow, A. W.; Shirk, J. S.; Pong, G. S. *J. Porphyrins Phthalocyanines* **2001**, 5, 582–592.
- (17) Pop, D.; Winter, B.; Freyer, W.; Hertel, I. V.; Widdra, W. *J. Phys. Chem. B* **2003**, 107, 11643–11647.
- (18) Pop, D.; Winter, B.; Freyer, W.; Widdra, W. J.; Hertel, I. V. *J. Phys. Chem. B* **2004**, 108, 9158–9167.
- (19) Pop, D.; Winter, B.; Freyer, W.; Widdra, W. J.; Hertel, I. V. *J. Phys. Chem. B* **2005**, 109, 7826–7833.
- (20) Firey, P. A.; Ford, W. E.; Sounik, J. R.; Kenney, M. E.; Rodgers, M. A. J. *J. Am. Chem. Soc.* **1988**, 110, 7626–7630.
- (21) Pelliccioli, A. P.; Henbest, K.; Kwag, G.; Carvagno, T. R.; Kenney, M. E.; Rodgers, A. J. *J. Phys. Chem. A* **2001**, 105, 1757–1766.
- (22) Anula, H. M.; Berlin, J. C.; Wu, H.; Li, Y.-S.; Peng, X.; Kenney, M. E.; Rodgers, M. A. J. *J. Phys. Chem. A* **2006**, 110, 5215–5223.
- (23) Rogers, J. E.; Nguyen, K. A.; Hufnagle, D. C.; McLean, D. G.; Su, W.; Gossett, K. M.; Burke, A. R.; Vinogradov, S. A.; Pachter, R.; Fleitz, P. A. *J. Phys. Chem. A* **2003**, 107, 11331–11339.
- (24) Calvete, M. J. F.; Dini, D.; Flom, R. S.; Hanack, M.; Pong, R. G. S.; Shirk, J. S. *Eur. J. Org. Chem.* **2005**, 3499–3509.
- (25) Marino-Ochoa, E.; Palacios, R.; Kodis, G.; Macpherson, A.; Gillbro, T.; Gust, D.; Moore, T. A.; Moore, A. L. *Photochem. Photobiol.* **2002**, 76, 116–121.
- (26) Dunlap, B. I.; Connolly, J. W. D.; Sabin, J. R. *J. Chem. Phys.* **1979**, 71, 3396–3402.
- (27) Baerends, E. J.; Ellis, D. E.; Ros, P. *Chem. Phys.* **1973**, 2, 41–51.
- (28) Salahub, D. R.; Fournier, R.; Mlynarski, P.; Papai, I.; St-Amant, A.; Ushio, J. In *Density Functional Methods in Chemistry*; Labanowski, J., Andzelm, J., Eds.; Springer-Verlag: New York, 1991; pp 77–100.
- (29) Gross, E. K. U.; Kohn, W. *Adv. Quantum Chem.* **1990**, 21, 255.
- (30) Casida, M. E.; Jamorski, C.; Casida, K. C.; Salahub, D. R. *J. Chem. Phys.* **1998**, 108, 4439–4449.
- (31) Nguyen, K. A.; Day, P. N.; Pachter, R. *J. Chem. Phys.* **1999**, 110, 9135–9144.
- (32) Ricciardi, G.; Rosa, A.; Baerends, E. J. *J. Phys. Chem. A* **2001**, 105, 5242–5254.
- (33) Liao, M.-S.; Watts, J. D.; Huang, M.-J. *Inorg. Chem.* **2004**, 44, 1941–1949.
- (34) Wu, D.-S.; Cheng, W.-D.; Li, X.-D.; Lan, Y.-Z.; Chen, D.-G.; Zhang, Y.-C.; Zhang, H.; Gong, Y.-J. *J. Phys. Chem. A* **2004**, 118, 1837–1843.
- (35) Liao, M.-S.; Watts, J. D.; Huang, M.-J.; Gorun, S. M.; Kar, T.; Scheiner, S. J. *Chem. Theory. Comput.* **2005**, 1, 1201–1210.
- (36) Zhang, Y.; Zhang, X.; Liu, Z.; Bian, Y.; Jiang, J. *J. Phys. Chem. A* **2005**, 109, 6363–6370.
- (37) Gunaratne, T. C.; Gusev, A. V.; Peng, X.; Rosa, A.; Ricciardi, G.; Baerends, E. J.; Rizzoli, C.; Kenney, M. E.; Rodgers, M. A. J. *J. Phys. Chem. A* **2005**, 109, 2078–2089.
- (38) Nguyen, K. A.; Day, P. N.; Pachter, R. *J. Phys. Chem. A* **2000**, 104, 4748–4754.
- (39) Kyrchenko, A.; Andreasson, J.; Martensson, J.; Albinsson, B. *J. Phys. Chem. B* **2002**, 106, 12613–12622.
- (40) Gouterman, M.; Wagniere, G. H.; Snyder, L. C. *J. Mol. Spectrosc.* **1963**, 11, 108.
- (41) Toyota, K.; Hasegawa, J.; Nakatsuji, H. *J. Phys. Chem. A* **1997**, 101, 446–451.
- (42) Baerends, E. J.; Ricciardi, G.; Rosa, A.; van Gisbergen, S. J. A. *Coord. Chem. Rev.* **2002**, 230, 5–27.
- (43) Delley, B. *J. Chem. Phys.* **2000**, 113, 7756–7764.
- (44) Schmidt, M. W.; Baldridge, K. K.; Boatz, J. A.; Elbert, S. T.; Gordon, M. S.; Jensen, J. H.; Koseki, S.; Matsunaga, N.; Nguyen, K. A.; Su, S.; Windus, T. L.; Dupuis, M.; Montgomery, J. A. *J. Comput. Chem.* **1993**, 14, 1347–1363.

- (45) Frisch, M. J.; Trucks, G. W.; Schlegel, H. B.; Scuseria, G. E.; Robb, M. A.; Cheeseman, J. R.; Montgomery, J. A., Jr.; Vreven, T.; Kudin, K. N.; Burant, J. C.; Millam, J. M.; Iyengar, S. S.; Tomasi, J.; Barone, V.; Mennucci, B.; Cossi, M.; Scalmani, G.; Rega, N.; Petersson, G. A.; Nakatsuji, H.; Hada, M.; Ehara, M.; Toyota, K.; Fukuda, R.; Hasegawa, J.; Ishida, M.; Nakajima, T.; Honda, Y.; Kitao, O.; Nakai, H.; Klene, M.; Li, X.; Knox, J. E.; Hratchian, H. P.; Cross, J. B.; Bakken, V.; Adamo, C.; Jaramillo, J.; Gomperts, R.; Stratmann, R. E.; Yazyev, O.; Austin, A. J.; Cammi, R.; Pomelli, C.; Ochterski, J. W.; Ayala, P. Y.; Morokuma, K.; Voth, G. A.; Salvador, P.; Dannenberg, J. J.; Zakrzewski, V. G.; Dapprich, S.; Daniels, A. D.; Strain, M. C.; Farkas, O.; Malick, D. K.; Rabuck, A. D.; Raghavachari, K.; Foresman, J. B.; Ortiz, J. V.; Cui, Q.; Baboul, A. G.; Clifford, S.; Cioslowski, J.; Stefanov, B. B.; Liu, G.; Liashenko, A.; Piskorz, P.; Komaromi, I.; Martin, R. L.; Fox, D. J.; Keith, T.; Al-Laham, M. A.; Peng, C. Y.; Nanayakkara, A.; Challacombe, M.; Gill, P. M. W.; Johnson, B.; Chen, W.; Wong, M. W.; Gonzalez, C.; Pople, J. A. *Gaussian 03, Revision C.02*; Gaussian, Inc.: Wallingford, CT, 2004.
- (46) Perdew, J. P.; Burke, K.; Ernzerhof, M. *Phys. Rev. Lett.* **1996**, *77*, 3865–3868; **1997**, *78*, 1396–1396.
- (47) Delley, B. *J. Chem. Phys.* **1990**, *92*, 508–517.
- (48) Francl, M. M.; Petro, W. J.; Hehre, W. J.; Binkley, J. S.; Gordon, M. S.; DeFrees, D. J.; Pople, J. A. *J. Chem. Phys.* **1982**, *77*, 3654–3665.
- (49) Becke, A. D. *J. Chem. Phys.* **1993**, *98*, 5648–5652.
- (50) Stratmann, R. E.; Scuseria, G. E.; Frisch, M. J. *J. Chem. Phys.* **1998**, *109*, 8128–8224.
- (51) Baker, J.; Scheiner, A.; Andzelm, J. *Chem. Phys. Lett.* **1993**, *216*, 380.
- (52) Petit, L.; Quartarolo, A.; Adamo, C.; Russo, N. *J. Phys. Chem. B* **2006**, *110*, 2398–2404.
- (53) Infante, I.; Lelj, F. *Chem. Phys. Lett.* **2003**, *367*, 308–318.
- (54) Dreuw, A.; Head-Gordon, M. *Chem. Rev.* **2005**, *105*, 4009–4037.
- (55) Ridley, J.; Zerner, M. *Theor. Chim. Acta* **1973**, *32*, 111–134.
- (56) Zhou, X.; Ren, A.-M.; Feng, J.-K.; Liu, X.-J. *Can. J. Chem.* **2004**, *82*, 19–26.
- (57) Chen, L. X.; Shaw, G. B.; Tiede, D. M.; Zuo, X.; Zapol, P.; Redfern, P. C.; Curtiss, L. A.; Sooksimuang, T.; Mandal, B. K. *J. Phys. Chem. B* **2005**, *109*, 16598–16609.
- (58) Hirshfeld, F. L. *Theor. Chim. Acta B* **1977**, *44*, 129.
- (59) Mulliken, R. S. *J. Chem. Phys.* **1955**, *23*, 1833.
- (60) Roy, R. K.; Bagaria, P.; Naik, S.; Kavala, V.; Patel, B. K. *J. Phys. Chem. A* **2006**, *110*, 2181–2187.
- (61) To be published in the ARL Technical Report.
- (62) Mooney, J. R.; Choy, C. K.; Knox, K.; Kenney, M. E. *J. Am. Chem. Soc.* **1975**, *97*, 3033–3038.
- (63) Wheeler, B. L.; Nagasubramanian, G.; Bard, A. J.; Schechtman, L. A.; Dininny, D. R.; Kenney, M. E. *J. Am. Chem. Soc.* **1984**, *106*, 7404–7410.
- (64) Petit, L.; Quartarolo, A.; Adamo, C.; Russo, N. *J. Phys. Chem. B* **2006**, *110*, 2398–2404.
- (65) Orti, E.; Piqueras Cresp, R.; Bredas, J. L. *Chem. Mater.* **1990**, *2*, 110–116.

CT700017B